

RESEARCH

Open Access



Fabrication of apigenin and adenosine-loaded nanoparticles against doxorubicin-induced myocardial infarction by reducing inflammation and oxidative stress

Ruixuan Li¹, Aixia Xu², Ye Chen¹, Yihui Li¹, Ru Fu¹, Weihong Jiang^{1*} and Xiaogang Li^{1*}

Abstract

The study's goals are to fabricate PLGA nanoparticles (PNPs) loaded with apigenin (AP) and adenosine (AD) using a microfluidic preparation method to a standard emulsification method and investigate the possible heart-protective effects of AP-AD PNPs made using the emulsification method. Compared to microfluidics, the emulsification method fabricated small-size nanoparticles, which are better at encapsulating drugs, retaining more drugs, and having a low viscosity for the myocardial infarction (MI) injection. The MI model was developed using SD rats injected under the skin with 85 mg/kg doxorubicin (DOX) for 2 days. The metabolic results showed that our AP-AD PNPs accelerated the blood flow in rats with MI, which increased the amounts of AP and AD in the circulatory system. This led to significant improvements in the cardiac index and lower amounts of AST, LDH, and CK in the blood. A histopathological study using Hematoxylin&eosin, and TUNEL staining showed that cardiac function had improved and apoptosis had decreased. Moreover, tests that checked the amounts of IL-6, TNF- α , NO, GSH, MDA, and SOD showed that AP-AD PNPs may help treat MI by reducing oxidative stress and inflammation, making it a potentially useful therapeutic approach.

Keywords Myocardial infarction, Apigenin, Adenosine, PLGA nanoparticles, Nanomedicine, Emulsification method

Introduction

Ischemic heart disease, as stated by the World Health Organization, is the primary cause of death globally, with myocardial infarction (MI) being the most severe clinical manifestation of this condition [1]. Enhancing strategies for preventing the onset of MI and ensuring prompt and efficient treatment are of utmost significance. Thrombolytic therapy or direct percutaneous coronary intervention performed promptly after an MI, followed by administering lipid-lowering drugs and anti-coagulants, are the most effective treatment approaches for MI patients [2]. These interventions have been shown to significantly decrease the size of the heart attack and reduce mortality rates [3]. Percutaneous coronary intervention

*Correspondence:

Weihong Jiang
jwhdoc@outlook.com
Xiaogang Li
hnxyxg@csu.edu.cn

¹Department of Cardiology, The Third Xiangya Hospital of Central South University, Changsha 410013, China

²Department of Endocrinology, Changsha Central Hospital, Changsha 410007, China



© The Author(s) 2024. **Open Access** This article is licensed under a Creative Commons Attribution-NonCommercial-NoDerivatives 4.0 International License, which permits any non-commercial use, sharing, distribution and reproduction in any medium or format, as long as you give appropriate credit to the original author(s) and the source, provide a link to the Creative Commons licence, and indicate if you modified the licensed material. You do not have permission under this licence to share adapted material derived from this article or parts of it. The images or other third party material in this article are included in the article's Creative Commons licence, unless indicated otherwise in a credit line to the material. If material is not included in the article's Creative Commons licence and your intended use is not permitted by statutory regulation or exceeds the permitted use, you will need to obtain permission directly from the copyright holder. To view a copy of this licence, visit <http://creativecommons.org/licenses/by-nc-nd/4.0/>.

can reestablish blood flow in the obstructed coronary artery [4]. However, it is susceptible to ischemia-reperfusion (I/R) injury, which can cause additional tissue damage and apoptosis of myocardial cells [5]. Ultimately, this can result in the development of heart failure and other unfavourable outcomes. Furthermore, the body will experience many pathological alterations following an MI, including the generation of reactive oxygen species (ROS), impairment of mitochondrial function, excessive accumulation of calcium, and other mechanisms that lead to cell death and an inflammatory reaction. Despite discovering anti-inflammatory and antioxidant drugs, their effectiveness is limited due to a lack of targeting, low absorption, and short half-life. Hence, devising safer and more efficient approaches to prevent and treat MI is imperative [6–8].

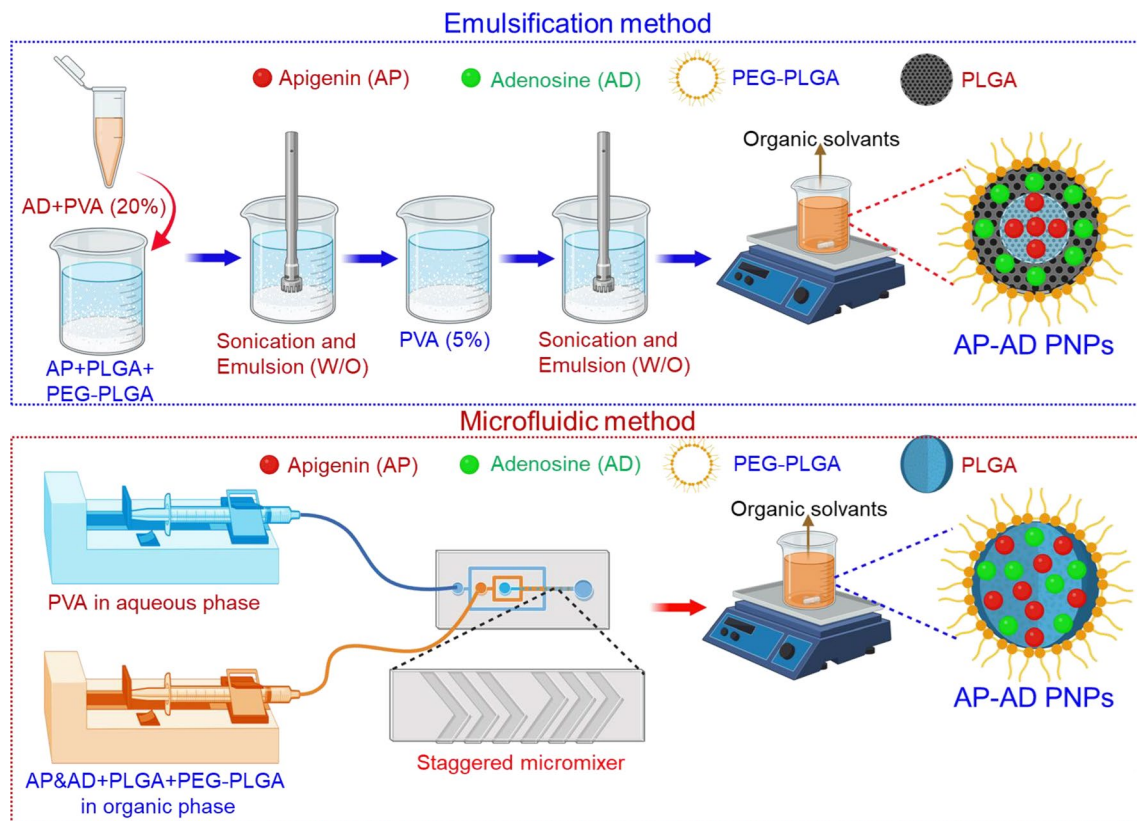
Nanoparticles are particles that have a size range of 1–100 nm. They are extensively utilized in medicine because of their diverse range of structures, sizes, forms, surface chemistry, and other characteristics [9]. Nanodelivery systems offer numerous advantages compared to conventional drug delivery systems, including diminished adverse effects, enhanced bioavailability, improved drug effectiveness, decreased drug dosage, prolonged administration duration, modified administration routes, and lowered treatment expenses [10]. This article concisely overviews commonly used carriers' physical and chemical characteristics, including polymer nanoparticles. It also discusses the progress and utilization of these nanoparticles in preventing and treating MI based on their underlying pathological mechanisms [11–14]. An approach to mitigate the hepatotoxicity and nephrotoxicity of TPL is to provide it locally in the heart through *in situ* injection, allowing for prolonged release. Polylactico-glycolic acid (PLGA) is a biodegradable copolymer that has received approval from the U.S. Food and Drug Administration (FDA) [15]. PLGA nanoparticles can encapsulate various drugs, enhancing their bioavailability and enabling controlled and prolonged drug release. Nevertheless, a drawback of PLGA nanoparticles is the possibility of drug burst release, which can lead to excessive and potentially hazardous drug release during the initial phase. Furthermore, the issue of whether these PLGA nanoparticles can remain in the myocardium is also a concern when using direct myocardial injection [16–18].

There is a greater emphasis on natural chemicals with distinctive chemical structures and specific pharmacological actions. Apigenin is a prevalent natural flavonoid found abundantly in vegetables and fruits, including parsley, celery, oranges, onions, honey, and others [19–21]. It is also present in plant beverages, such as tea and wine. Apigenin is considered more helpful due to its superior safety profile compared to other flavonoids regarding cellular health. Currently, there is limited evidence

indicating any adverse metabolic effects of apigenin. Apigenin exhibits antioxidant, anti-inflammatory, antiviral, and anticancer properties [22]. Furthermore, apigenin has a cardioprotective impact by safeguarding endothelial cell functionality, mitigating coronary atherosclerosis, and impeding diabetic myocardial harm. Apigenin has been found to protect against myocardial injury caused by oxidative stress. However, the exact mechanism of this protection has not been completely understood and requires additional exploration [23].

Adenosine has a crucial role as a signalling molecule in cells during conditions of reduced blood flow, controlling cellular metabolism and protecting cells from harm caused by low oxygen levels and oxidative stress [24]. There is a strong connection between MI and adenosine. Adenosine, ATP, and ADP are released during cellular or tissue hypoxia or ischemia and cause reactive hyperemia. Reactive hyperemia temporarily increases blood flow when blood arteries reopen after interrupted blood delivery to the tissues [25]. MI causes a lack of oxygen and blood supply to the heart tissue, releasing adenosine from cells. Adenosine then binds to adenosine receptors on the cell surface, resulting in a wide range of physiological effects. Research highlights the crucial significance of adenosine receptor A2AR in MI. The activation of A2AR controls the blood flow in the coronary artery, promoting blood circulation in the heart muscle tissue [26]. In addition, A1R counteracts reactive hyperemia, which is regulated by A2AR, thereby further regulating myocardial perfusion. Although there is an ongoing dispute regarding the involvement of adenosine in coronary reactive hyperemia, its significance in MI is extensively examined and recognized. However, several research have questioned the exact importance of adenosine in MI, suggesting that adenosine may not be a determining component in the development of MI [27]. The relationship between adenosine levels and the severity of MI is still unclear in many animal models and clinical research [28].

The work involved the development of AP-AD nanopreparations using PVA and PLGA as stabilizers and polymers. The emulsification and microfluidic system achieved this fabrication (Scheme 1). Subsequently, a comparison was made between the physical attributes of these nanopreparations with injectable PNPs. In addition, the pharmacodynamic and pharmacokinetic characteristics of AP-AD NPs, fabricated by emulsification, were examined in MI induced by doxorubicin (DOX). The efficacy in preventing MI was evaluated using multiple techniques, such as histological investigation and biochemical markers. This study investigated the possibility of nanopreparations as efficacious therapies for MI.



Scheme 1 Graphical representation of fabrication of AP-AD PNPs *via* emulsification and microfluidic technique

Materials and methods

Materials

Unless noted in the procedure, all chemicals were purchased from commercial suppliers and used without further purification. All aqueous solutions were prepared by using ultrapure water from a Milli-Q system. Apigenin (AP) was obtained from Alfa. Adenosine (AD) was obtained from AK Scientific. Polylactic acid-glycolic acid copolymer, poly(vinyl alcohol), and poly(ethylene glycol) methyl ether-block-poly(lactide-co-glycolide) were provided from Sigma Aldrich (St. Louis, USA). Dichloromethane (DCM) and methanol (MeOH) were acquired from Xi'an Ruixi Biological Technology Co., Ltd. Dialysis bag (MWCO 8000–14000 Da) was attained from Shanghai Macklin Biochemical Co., Ltd. Metoprolol tartrate (MT) injection was obtained from Bio Basic Inc. Doxorubicin (DOX) were purchased from Thermo Fisher Scientific. NO, GSH, MDA, SOD, AST, LDH, and CK were provided by BioLegend. IL-6 and TNF- α were purchased from Beyotime Biotechnology.

Preparation of AP-AD PNPs by emulsification method

AP-AD PNPs were synthesized using the emulsification technique [29]. The internal aqueous phase comprised 20 mg of AD immersed in 2 mL of 20% PVA. A solution of PEG-PLGA (8 mg) and PLGA (12 mg) polymers was

prepared by dissolving them in 3 mL of dichloromethane. This solution was combined with an AP (12 mg) solution, which served as the oil phase. The outer aqueous phase consisted of a polyvinyl alcohol (PVA) solution with a concentration of 5% in a total capacity of 20 mL. The oil and aqueous phases were combined in an ice-water bath and subjected to intermittent sonication for 5 min, with 3-second intervals every 5 s, to produce colostrum. The aqueous solution was introduced to the colostrum, producing a white colour solution. The solution was subjected to continuous stirring under a magnetic stirrer for 5 h, forming a stable system and facilitating the evaporation of the organic solvent.

Preparation of AP-AD PNPs by microfluidic system

The preparation of nanoparticles was carried out using a microfluidic device [30]. The ports were linked to the water phase holding the PVA solution (3.1%). The AP (12 mg) and AD (20 mg) solutions were effectively dissolved in MeOH (3 mL) using ultrasonic waves. Similarly, the PEG-PLGA and PLGA (3:7) were dissolved in 3 mL of acetonitrile. These solutions were then combined and linked as organic phases to additional ports. The flow ratio of the organic and aqueous phases was 1:3, and the flow ratio was 137 μ L/min. The NPs were retrieved from microfluidic output. Ultimately, they

underwent purification using ultracentrifugation and were de-frizzed.

Characterization of NPs

Transmission electron microscopy (TEM) images were attained using a JEOL 3011 transmission electron microscope with an accelerating voltage of 300 kV. The morphologies of the NPs were investigated using a field-emission scanning electron microscope (FE-SEM, TESCAN MIRA3, Czech Republic). Zeta potential and dynamic light scattering (DLS) were obtained on an Anton Paar Litesizer 500 particle analyzer.

Animals

Primarily, adult male SPF rats (weight, 200–250 g; 10–12 weeks old; SLRC Laboratory Animal, Shanghai, China) were used to perform various in vivo functional assessments. All animal procedures and protocols were approved by the animal centre of the Third Xiangya Hospital, Central South University and conformed to the “Guidelines for the Care and Use of Laboratory Animals” published by the U.S. NIH. The rats were anesthetized by inhalation of isoflurane and placed on a respirator during surgery to maintain ventilation. The MI model rats were randomly divided into five treatment groups: a fresh group (group I-sham, group II-model, group III-AP&AD mixtures (5 mg/kg for AP & 7.5 mg/kg for AD), group IV-AP-AD PNPs, and group V-MT injection). The cell onto the infarct area in the fresh and vitrification groups. In the sham-operation group, rats were subjected to thoracotomy. The effect of the transplantation of various sheets on cardiac function was evaluated. The rats were anesthetized by inhalation of isoflurane to alleviate suffering, and the hearts were quickly procured to determine further investigations.

Cardiac index and H&E staining

Rats were euthanized after MI, and the cardiac index of the hearts was harvested following a previously described method. The heart tissues were fixed in 4% paraformaldehyde solution after being washed by PBS, perfused with 30% sucrose at 4 °C overnight, and embedded in optimal cutting temperature compound for the frozen section. A Leica CM1950 cryostat was used to cut 5-mm sections in preparation for H&E staining analysis. The TUNEL (Roche) was performed on day 3 after I/R according to the kit manufacturer’s instructions [31], and the fluorescence intensity was calculated using ImageJ.

Assessment of cardiac marker enzymes

The rat blood was gathered from the jocular arteries following a 3-day treatment. After allowing the samples for 1–2 h, they were centrifuged, and the resulting serum was kept at -20 °C. A fluorescent ELISA microplate

reader measured the serum ratio of AST, CK, and LDH [32].

Biochemical serum analysis

The NO, MDA, GSH, and SOD ratio in the serum was noticed by ELISA kits measuring the IL-6 and TNF- α concentrations in serum [33].

Statistical analysis

Experiments were operated by members blinded to grouping information. The operators analyzed all data. Data acquired from each experiment was presented as mean \pm standard deviation (SD) from at least 3 independent repeats. Data from more than two groups was analyzed using one-way ANOVA or two-way ANOVA. *P*-value < 0.05 was considered statistically significant. GraphPad Prism (version: 9.0.0; GraphPad Prism Software Inc, San Diego, CA).

Results

Comparison of AP-AD PNPs developed by microfluidic to emulsion system

Figure 1A and B illustrate the UV-Vis spectral analysis of AP and AD in a methanolic solution. The peaks of AP were detected at 332 nm, while AD showed its band at 228 nm. The wavelengths of 332 and 228 nm were chosen for the analysis of AP and AD, respectively, using HPLC. To attain the highest EE and DL levels. The AP-AD PNPs were light-yellow, fabricated by emulsification (Fig. 1G) and microfluidic procedures (Fig. 1H), and then lyophilized.

Scanning electron microscopy (SEM) measurements of AP-AD PNPs are shown in (Fig. 1C and D). The AP-AD PNPs developed by the emulsion method display more difference in diameter and greater polydispersity than the microfluidic method, as the microfluidic method can deliver a homogenous distribution of AP-AD PNPs. Transmission electron microscopy (TEM) measurements (Fig. 1E and F) showed that both approaches produced spherical nanoparticles without adherence. The size of the hydrated particles of the nanoparticles fabricated by emulsification was less than that of those prepared through microfluidic methods (100.02 \pm 4.52 nm vs. 149.26 \pm 2.14 nm), which aligns with the observations made using TEM. In addition, the surface potentials of NPs fabricated using emulsion and microfluidic methods were measured to be -27.26 \pm 3.63 mV and -16.25 \pm 2.94 mV. According to Fig. 1G, AP-AD PNPs prepared using the emulsion method had higher encapsulation efficiency (AP: 80.87 \pm 2.57% vs. 79.61 \pm 2.01%, AD: 74.36 \pm 4.52% vs. 70.93 \pm 3.82%) and drug loading (AP: 0.88 \pm 0.02% vs. 0.48 \pm 0.02%, AD: 1.81 \pm 0.02% vs. 0.87 \pm 0.02%) compared to the microfluidic method. This suggests that

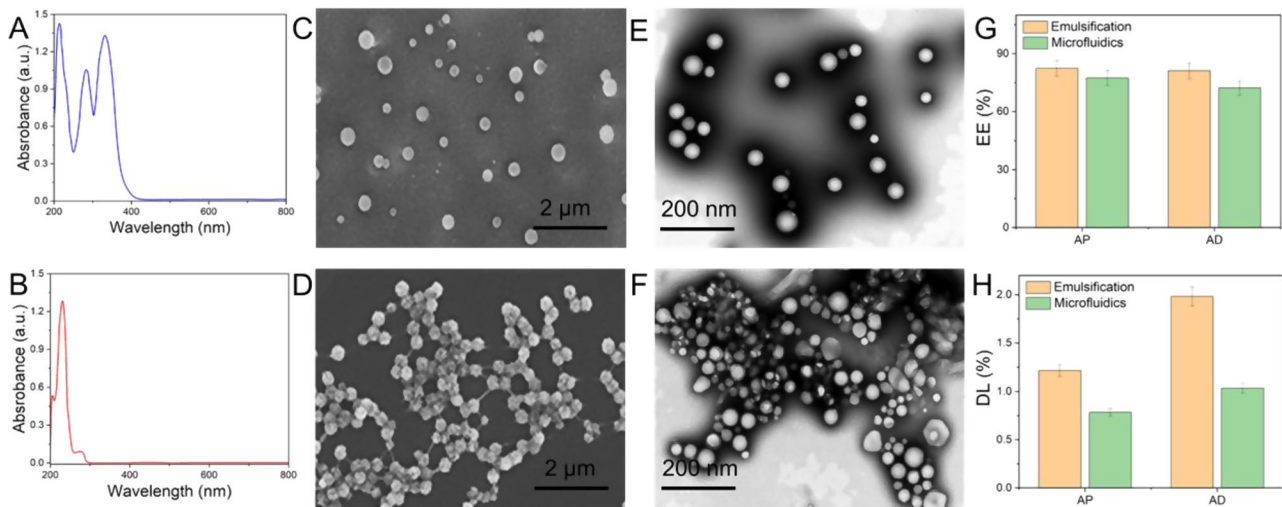


Fig. 1 **A** and **B**) Ultraviolet-visible spectroscopy (UV-Vis) spectra of apigenin (AP) and adenosine (AD) in methanolic solution. **C** and **D**) Scanning electron microscopy (SEM) images of AP-AD PNPs developed by emulsion and microfluidic technique. The scale bar is 2 μ m. **E** and **F**) Transmission electron microscopy (TEM) images of AP-AD PNPs developed by emulsion and microfluidic technique. The scale bar is 200 nm. **G** and **H**) EE and DL of AP-AD PNPs developed by emulsion and microfluidic technique. Data are presented as mean \pm standard deviation (SD) ($n=3$)

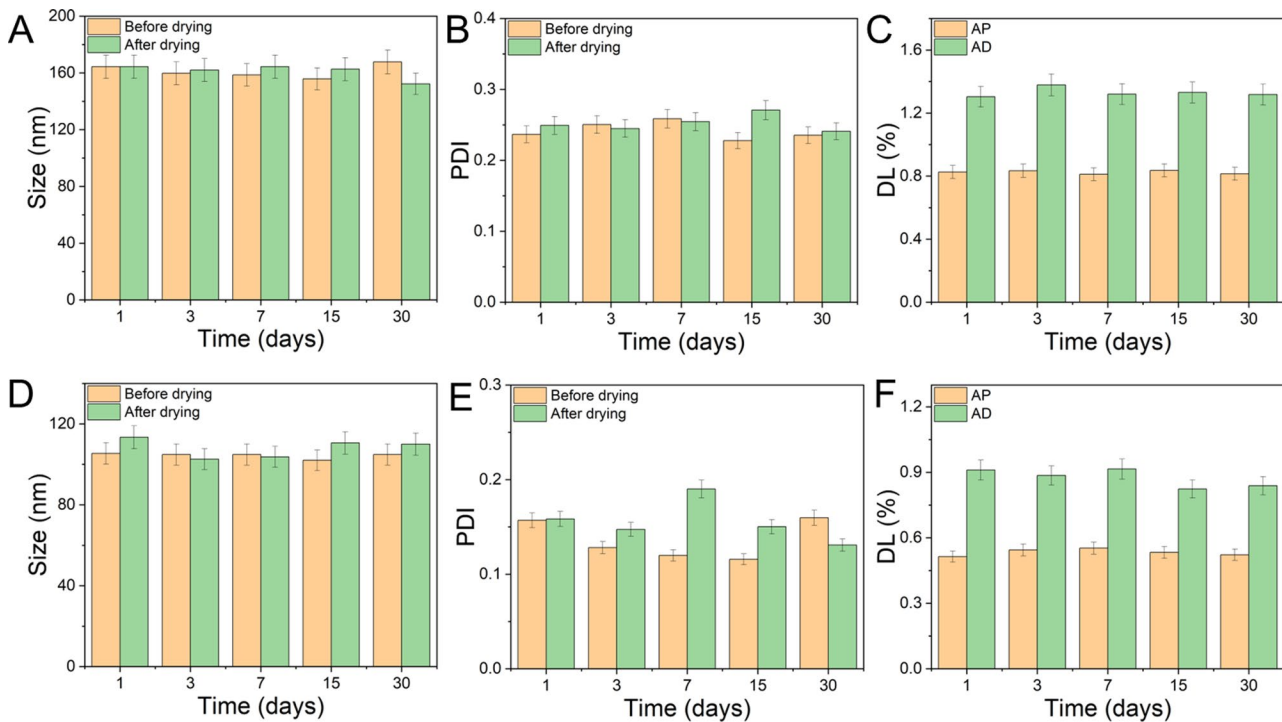


Fig. 2 The hydrodynamic size, polydispersity index (PDI), and drug loading (DL) changes of AP-AD PNPs developed by emulsion (**A-C**) and microfluidic technique (**D-F**). Data are presented as mean \pm standard deviation (SD) ($n=3$)

the emulsion technique is superior to the microfluidic method for AP-AD PNPs.

The stability of the AP-AD PNPs over 30 days was examined by monitoring the variations in hydrodynamic size, polydispersity index (PDI), and drug loading. The diameter and polydispersity index of AP-AD PNPs showed minor fluctuations (<11%) over 30 consecutive days, both during emulsification and microfluidics

processes (Fig. 2A and C). Additionally, the variations in their drug loading (DL) were less than 6% and 11%, respectively (Fig. 2D and F). Both AP-AD PNPs were constant for 30 days.

To evaluate the suitability of AP-AD PNPs for intravenous injection in animal trials, the relative viscosity of the samples was assessed using an unbeloved viscometer in water. This comparison was done in two different ways,

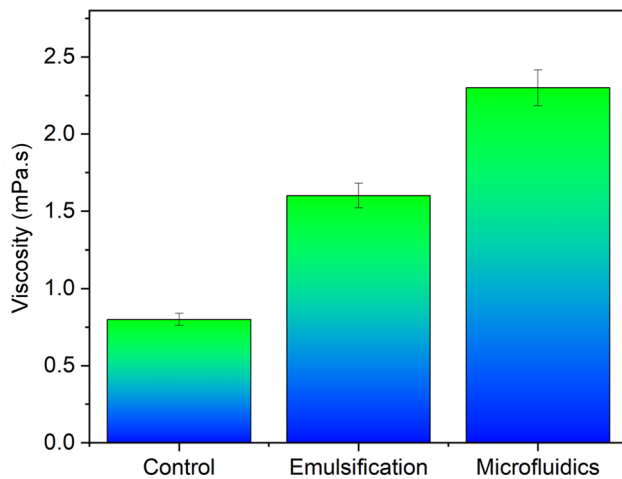


Fig. 3 Investigation of viscosity of AP-AD PNPs. Data are presented as mean \pm standard deviation (SD) ($n=3$)

and the results are presented in Fig. 3. The mixture of AP and AD served as the control, while the nanoparticles fabricated using both procedures exhibited a high viscosity. The emulsion approach fabricated nanoparticles with lower viscosity compared to the microfluidic method. Injecting nanoparticles intravenously offered significant benefits in lowering injection pressure.

In vitro drug release of AP-AD PNPs

Figure 4A and B illustrate the drug release patterns of the AP-AD PNPs fabricated using the emulsion and microfluidic method compared to the release of AP and AD. The release of AD from AP-AD PNPs exhibited a release pattern that closely resembled that of the unbound drug. The significant amount of AD adhesion on the PLGA NP surface is believed to be a substantial factor in the similar release profile observed between AP-AD PNPs and AP and AD. When water enters the polymer matrix, AD quickly dissolves, spreads, and is released into areas with

lower concentrations. Nevertheless, the AP in AP-AD PNPs demonstrated a swift initial discharge in the first 4 h and 8 h for emulsion and microfluidic method, by a continuous release for 20 h. Conversely, the distribution of complimentary AP was rapid and concluded at 6 h. The earlier investigation also noted a comparable pattern. The AP release in the AP-AD PNPs obtained using the emulsion method consistently exceeded that in the microfluidic method, likely because of the increased drug loading. The initial fast release of the drugs was mainly caused by the drug being absorbed onto the surface of the PNPs.

AP-AD PNPs elevated the AP and AD levels in MI

In this work, the concentrations of AP and AD were evaluated using the UPLC-MS/MS method following intravenous administration of a mixture of AP and AD, as well as AP-AD PNPs, in rats having MI. The measured concentrations were then plotted against the relevant time points. Figure 5A and B display the graph depicting the relationship between plasma concentration and time. The area under the concentration-time curve (AUC) of AP and AD increased approximately 3.5 times in the AP-AD PNPs than AP&AD (AP: 3.19 ± 0.80 vs. 0.91 ± 0.15 h \times μ g/mL; AD: 81.58 ± 20.87 vs. 24.21 ± 1.96 h \times μ g/mL). This suggests that there was a greater concentration of AP and AD in the serum (AP: 5.11 ± 1.93 vs. 1.98 ± 0.50 μ g/mL; AD: 140.36 ± 29.63 vs. 29.63 ± 7.41 μ g/mL) and a longer blood flow (AP: 2.69 ± 0.52 vs. 0.93 ± 0.40 h; AD: 2.59 ± 0.52 vs. 0.79 ± 0.12 h). The CL_z of AP and AD reduced by three times in the AP-AD PNPs compared to the AP&AD (AP: 1.57 ± 0.35 vs. 5.60 ± 0.72 L/h/kg; AD: 0.11 ± 0.03 vs. 0.29 ± 0.02 L/h/kg). This confirms that AP-AD PNPs are more stable than AP&AD and may lead to improved therapeutic outcomes. These outcomes essentially agree with existing research that demonstrates an extended duration of drug presence

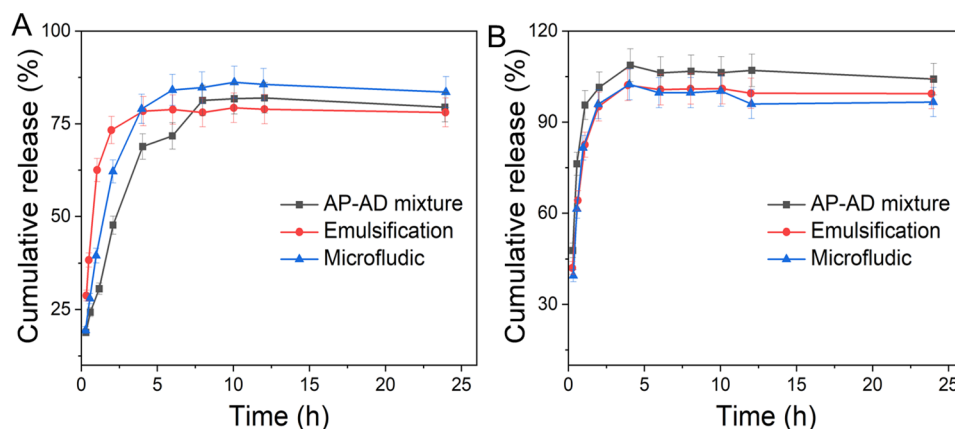


Fig. 4 In vitro AP and AD release pattern of AP-AD PNPs. (A) AP release pattern of AP-AD PNPs. (B) AD release pattern of AP-AD PNPs. Data are presented as mean \pm standard deviation (SD) ($n=3$)

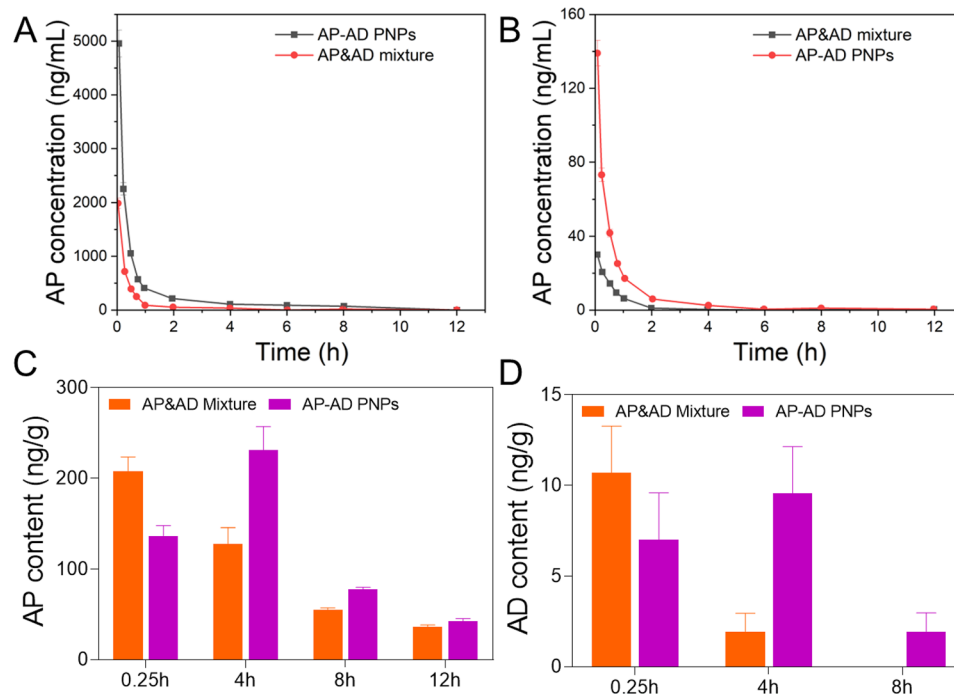


Fig. 5 Plasma outlines and heart ratio in intravenously injected MI rats with AP&AD mixtures and AP-AD PNPs. **A** and **B**) AP and AD plasma concentrations versus time profile. **C** and **D**) The levels of AP and AD in the heart were observed at different hours. Data are presented as mean \pm standard deviation (SD) ($n=3$)

in the bloodstream following the encapsulation of nanoparticles.

To confirm the targeted organs' drug concentration, we examined the particular amounts of AP and AD in the heart, as depicted in Fig. 5C and D. However, the concentrations of AP-AD PNPs were lesser than their AP&AD at 0.25 h. As anticipated, the concentration of AP and AD in the heart, when delivered through AP-AD PNPs, was 1.6 times and 17.2 times higher than that in the AP&AD after 4 h. This finding proves that encapsulating AP and AD in nanoparticles enhances their stability *in vivo*. Moreover, it suggests that the targeted delivery of AP and AD to the affected tissue can lead to improved and simplified treatment of MI.

AP-AD PNPs improved AP and AD accumulation in the MI model

Figure 6A-H demonstrate that AP and AD may be identified in many organs following intravenous injection, suggesting a broad dispersion throughout the body. The distribution of AP was primarily observed in the kidney, liver, heart, and brain. On the other hand, AD was found to be distributed in the heart, brain, liver, and kidney. AP and AD were promptly disseminated upon intravenous injection at 0.25 h, with the AP and AD concentrations in each tissue being usually higher in the AP&AD compared to the nanopreparations group. The free AP and AD molecules experienced constant degradation and elimination

in the body within 0.25 h due to their inherent instability, reducing their presence in the tissues. Elevated levels of AP and AD in the liver and kidneys contribute to increased blood circulation in these organs.

AP-AD PNPs can reverse the histopathology variation in the MI model

Figure 7 depicts the histological changes detected in the hearts after the therapy. The cardiac slice of negative control had a typical myofibril without any apparent abnormalities. In contrast, the model group had clear signs of fibrous tissue growth, necrosis, and myocardial fibrosis. The other groups showed a decrease in these abnormal structural alterations, while the AP-AD PNPs experienced a notable reduction in lesions. These findings indicate that the AP-AD PNPs were more effective in treating MI in the AP&AD combination.

AP-AD PNPs reduced the cell death of MI

The TUNEL labelling technique was employed to validate the presence of apoptosis in the cardiac tissue (Fig. 7). The outcomes of quantitatively analyzing cell death in the three rats in all the groups are displayed in Fig. 7. The TUNEL-stained cardiac sections of the negative control group exhibited a minimal presence of apoptotic cells ($0.31 \pm 0.56\%$), indicating a near absence of heart damage. As anticipated, a higher percentage of positive cells ($21.36 \pm 0.05\%$) was detected in the rats

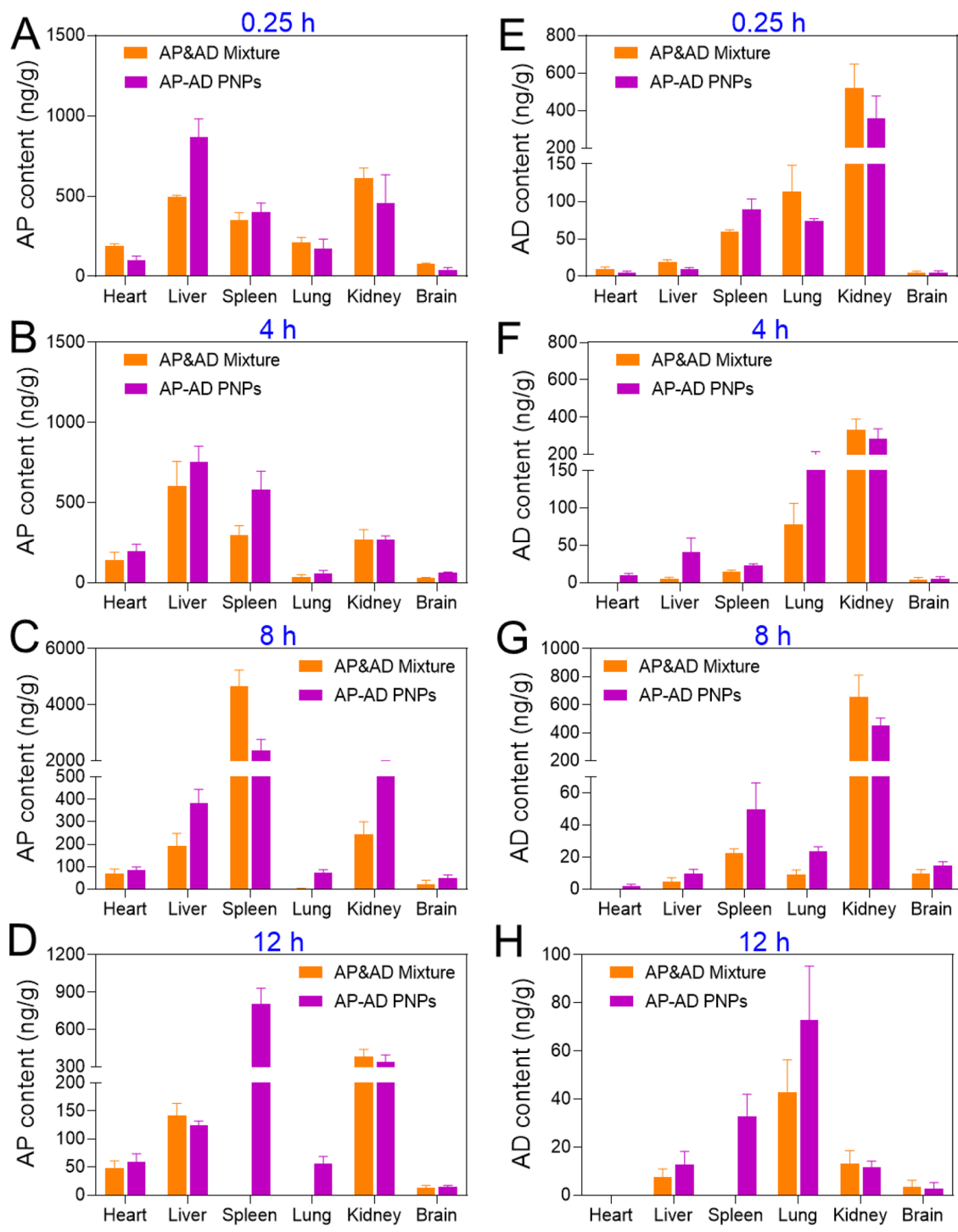


Fig. 6 Biodistribution of (A-D) AP and (E-H) AD in different organs at various hours. UPLC-MS/MS noted the levels of AP and AD in rat organs. Data are presented as mean ± standard deviation (SD) (n = 3)

with MI that were treated with saline. It is essential to mention that in MI rats administrated with an AP&AD (11.89 ± 1.67%), AP-AD PNPs (1.18 ± 0.39%), or MT injection (3.93 ± 0.52%), there was a significant decrease in the number of TUNEL positive cells. Significantly, the rate of cell death (apoptosis) in MI rats treated with AP-AD

PNPs was lower than that of those treated with the AP&AD mixture and MT injection. This finding further confirms that our AP-AD PNPs have a superior ability to prevent cell death and provide more excellent protection for MI rats.

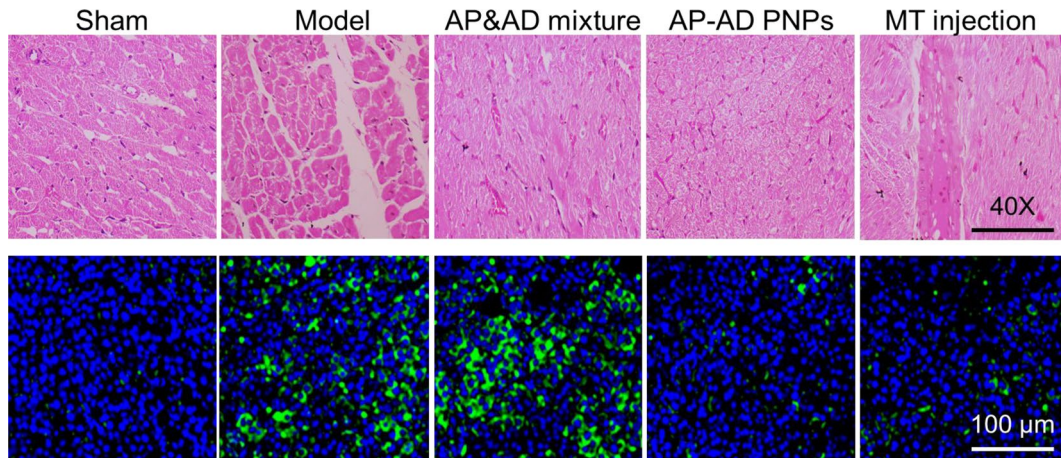


Fig. 7 AP-AD PNP inverted the histological variations in heart tissue after MI. Representative images of heart stained with H&E in sham, model, AP&AD mixtures, AP-AD PNP, and MT injection. The scale bar is 40 X (magnification). TUNEL in sham, model, AP&AD mixtures, AP-AD PNP, and MT injection. The scale bar is 100 μm

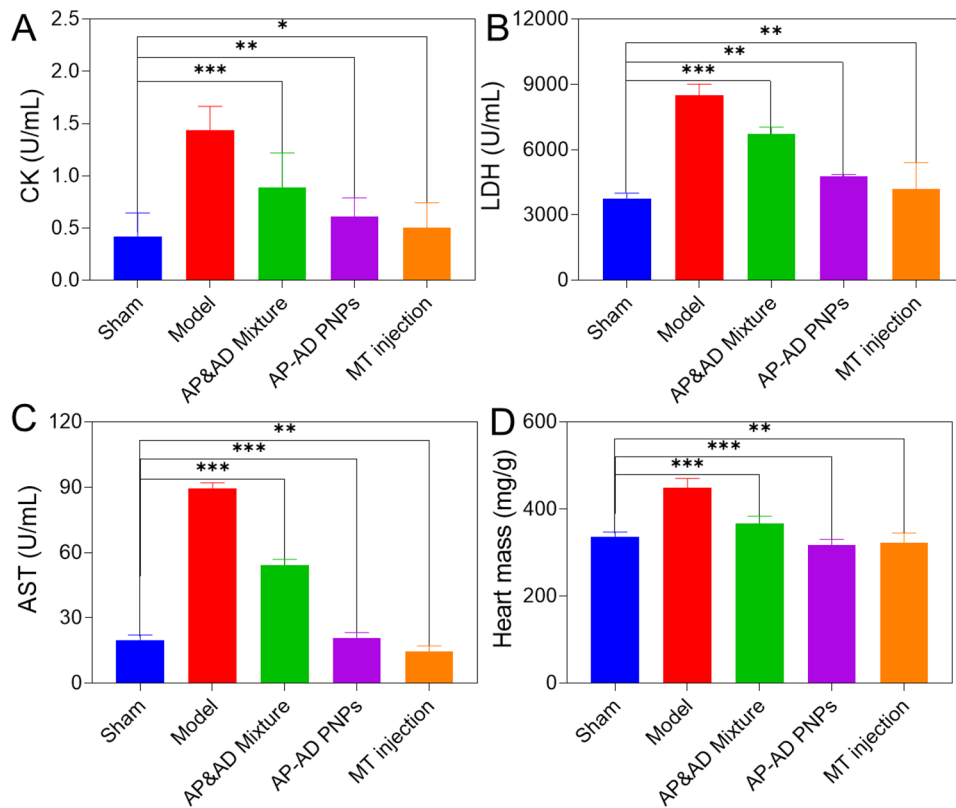


Fig. 8 Effects of AP-AD PNP on cardiac markers. (A) CK activity, (B) LDH activity, (C) AST activity, and (D) Heart mass in the serum. Data are presented as mean ± standard deviation (SD) (n = 6). *Compared with the control group (*P < 0.05, **P < 0.001, and ***P < 0.01)

Myocardial enzyme levels

Myocardial damage was assessed by analyzing serum cardiac biomarkers AST, LDH, and CK (Fig. 8A). The model group substantially increased AST (Fig. 8C), LDH (Fig. 8B), and CK serum levels. When the rats were treated with a combination of AP&AD, AP-AD PNP, and MT injection, their serum AST, LDH, and CK levels

showed partial recovery compared to the model group. Consistent with previous findings, the AP-AD PNP demonstrated the most effective inhibition of AST, LDH, and CK serum levels, suggesting that AP-AD PNP possess a favourable anti-MI property.

AP-AD PNPs enhanced the cardiac index

Figure 8D demonstrates notable variations in heart coefficient between the control and AP&AD and AP-AD PNPs. The heart experienced hypertrophy due to DOX administration, resulting in decreased body weight and a considerable increase in cardiac index. The cardiac index of rats significantly increased following the administration of a combination of AP&AD, AP-AD PNPs, and MT. Additionally, administering AP-AD PNPs and MT injections enhanced the cardiac index to an average level.

AP-AD PNPs can reduce oxidative stress

Figure 9A and D illustrate the impact of AP-AD PNPs on the levels of NO, MDA, GSH, and SOD in MI. The serum levels of GSH and SOD in the model group exhibited a significant drop, but the concentrations of MDA and NO showed a marked increase. Compared to the control group, the treatment with AP&AD mixture, AP-AD PNPs, and MT injection led to increased activities of GSH and SOD, as well as reduced levels of MDA and NO. In addition, AP-AD PNPs can greatly enhance GSH and SOD activities while decreasing MDA levels in rat serum, as compared to the AP&AD. The results indicated that AP-AD PNPs mitigated heart damage by activating the anti-oxidative system.

AP-AD PNPs can improve the inflammatory factor

The anti-inflammatory efficacy of AP-AD PNPs was assessed, as depicted in Fig. 10A and B. The presence of inflammatory factors, such as IL-6 and TNF- α , significantly influences the occurrence of MI. The levels of IL-6 and TNF- α in the serum of the model groups were increased considerably. Nevertheless, the combination of AP&AD, AP-AD PNPs, and MT injection group can decrease the activity of IL-6 and TNF- α . As anticipated, AP-AD PNPs can effectively decrease IL-6 and TNF- α levels in serum compared to the AP&AD. This indicates that AP-AD PNPs have lower anti-inflammatory properties.

The safety assessment of AP-AD PNPs

Figure 11 demonstrates that AP-AD PNPs accumulated in multiple organs, including the heart, liver, kidney, and brain. Subsequently, there was a steady process of hydrolysis and degradation. Therefore, to evaluate the safety of AP-AD PNPs, the organs from rats were removed and subjected to H&E staining after treatment. Figure 11 shows H&E pictures of normal rats exhibiting typical cell architecture. In contrast, Fig. 11 displays the hearts of model rats, where myocardial fibre necrosis and inflammation are evident. Histopathological examination of

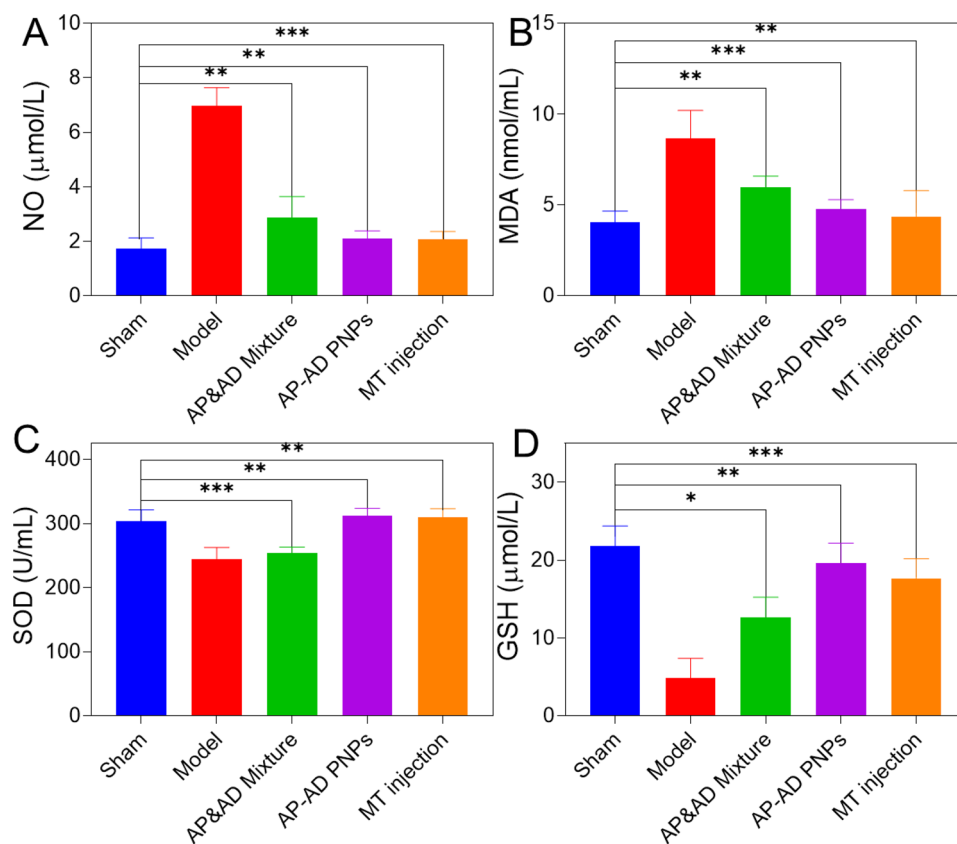


Fig. 9 AP-AD PNPs diminished the oxidative stress. **(A)** NO content, **(B)** MDA content, **(C)** SOD activity, and **(D)** GSH content. Data are presented as mean \pm standard deviation (SD) ($n=6$). *Compared with the control group (* $P < 0.05$, ** $P < 0.001$, and *** $P < 0.01$)

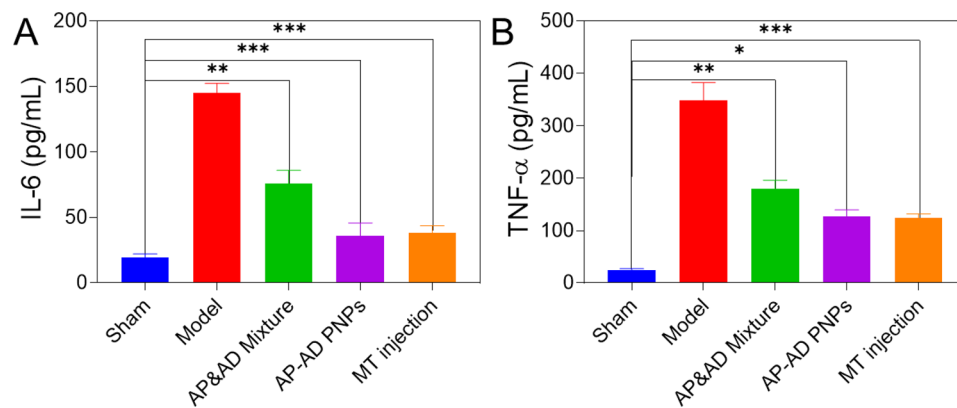


Fig. 10 AP-AD PNP improved the inflammatory factors. **(A)** IL-6 contents, and **(B)** TNF- α content. Data are presented as mean \pm standard deviation (SD) ($n=6$). *Compared with the control group (* $P < 0.05$, ** $P < 0.001$, and *** $P < 0.01$)

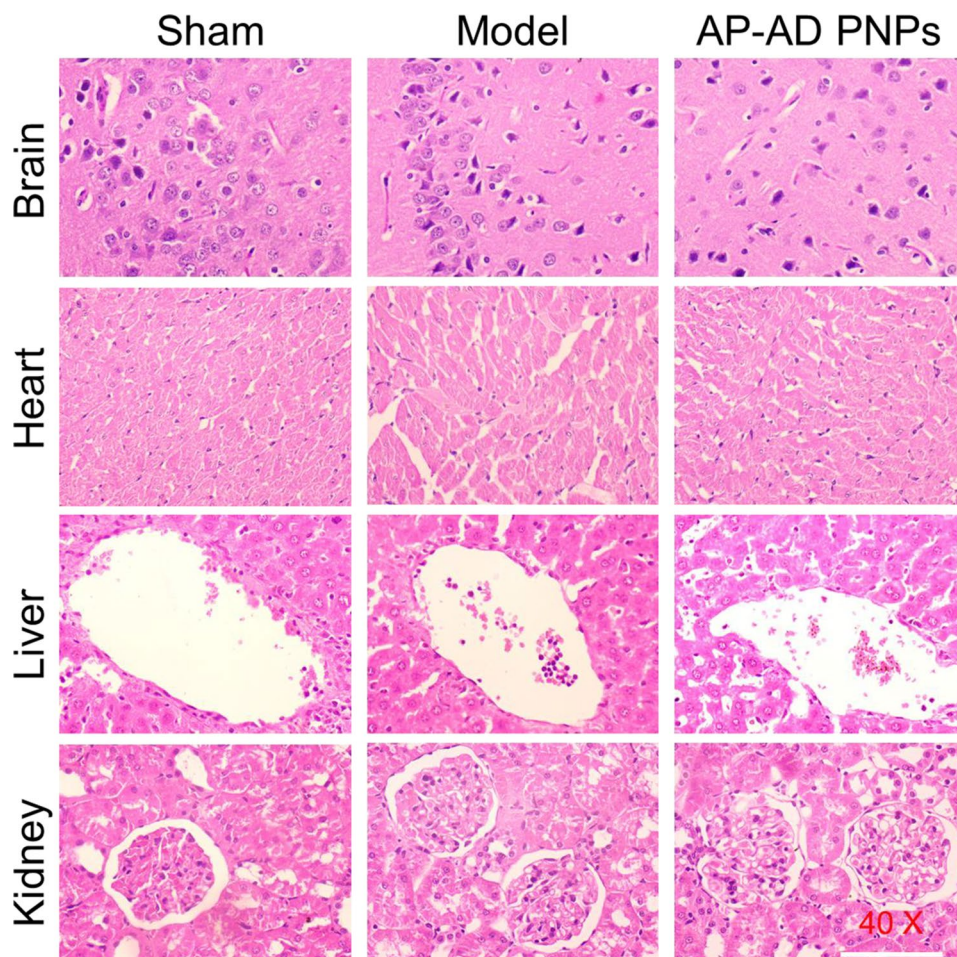


Fig. 11 Representative images of organs stained with H&E in sham, model and AP-AD PNP groups. The scale bar is 40 X (magnification)

model rats administrated with AP-AD PNP revealed unaltered cell morphology and the absence of any noticeable alterations compared to the control rats. This suggests that AP-AD PNP do not exhibit any evident *in vivo* toxicity.

Discussion

Percutaneous coronary intervention and thrombolysis are commonly employed in the treatment of MI. Nevertheless, the occurrence rate and death rate associated with this condition remain elevated [34–36]. Pursuing efficient natural remedies for cardiovascular ailments

is appealing due to their inherent safety. Reports are indicating that AP and AD can be utilized as treatment options for MI. Nevertheless, AP and AD were swiftly eliminated from biological systems due to their short half-life, which limited their accumulation in organisms [37–39]. The nanotechnology-based delivery approach mitigates several constraints and enhances bioavailability [11, 40, 41]. Hence, the drug delivery system was fabricated to use PLGA-encapsulated AP and AD to treat MI.

This work employed two different techniques, namely the emulsification and the microfluidic method, to encapsulate the medicines apigenin and adenosine. The double-emulsion process is commonly used to prepare PLGA NPs, enabling the simultaneous administration of medicines with hydrophobic and hydrophilic characteristics while ensuring a stable and compact shape. However, microfluidic technology has become a feasible alternative method due to the growing need to produce nanoparticles on a wide scale. This method provides multiple benefits, such as a more precise diameter distribution (lower PDI), improved EE and DL, decreased variances between batches, and the possibility of quickly scaling up to large-scale production. Based on our experimental findings, the emulsion nanoparticles fabricated demonstrated higher EE and DL, smaller particle size, and decreased viscosity. Nevertheless, TEM observation could not substantiate the theory due to its restricted resolution. In addition, different amounts of PVA were used in the two procedures to achieve similar encapsulation effectiveness and drug loading levels. Notably, PVA's viscosity also constrained the microfluidic process's overall flow rate. The flow rate peaked at 300 $\mu\text{L}/\text{min}$. As a result, this impeded the capacity to achieve uninterrupted manufacturing of nanoparticles on a significant scale. In this experiment, nanoparticles' continuous and extended production was prone to adhesion and obstruction at the mixing point on the chip. This compromised the chip's reusability and significantly increased the associated costs. Therefore, the emulsification technique was selected to prepare AP-AD PNPs in subsequent pharmacokinetic and pharmacodynamic studies.

DOX, a widely utilized drug, is regularly employed to intentionally cause MI damage both domestically and internationally [42]. Furthermore, administering excessive doses of DOX can result in MI and necrosis. Furthermore, the cardiac enzymes and histological abnormalities observed in the DOX-induced MI model closely resemble the pathological features typically shown in human MI [43]. Thus, the model chosen for this investigation was MI-induced by DOX in rats [44]. MT injection is primarily utilized in clinical settings as a β -adrenergic receptor blocker to prevent and treat MI, counteracting the MI induced by DOX. Therefore, MT injection was chosen as the medicine to be used as the positive control.

The cardiac profile and staining indicate the extent of damage to the cardiomyocytes. AST, LDH, and CK are classified as cardiac-enzyme markers. Consistent with expectations, the cardiac index was decreased, the tissue alterations were reversed, and the levels of myocardial enzymes were recovered following therapy.

Oxidative stress, inflammation, and apoptosis are key factors that regulate the advance of MI. Zhang et al. (2022) showed that scutellarin (SCU) protects against damage caused by cerebral ischemia-reperfusion in rats by decreasing inflammatory responses and oxidative stress through the MAPK/NF- κ B [42]. The analysis of oxidative stress markers (NO, MDA, GSH, and SOD) and inflammatory markers (IL-6 and TNF- α) demonstrated that after the administration of the treatment, there was a notable rise in GSH and SOD activity, along with a reduction in MDA and NO levels. As previously mentioned, the different treatment groups showed a decrease in the number of cells undergoing apoptosis in the heart tissue. It is important to note that the AP-AD PNPs had a considerably superior anti-apoptosis ability compared to the drug. (1) AP and AD can inhibit apoptosis. As supported by these studies, using PLGA enhanced the absorption and stability of AP and AD in the heart, and the ability to prevent cell death by apoptosis may also be strengthened. (2) The enhanced permeability and retention (EPR) phenomenon was also observed in the ischemic tissue. After undergoing MI, the EPR effect facilitated the accumulation of nanoparticles in the acutely injured tissue, leading to increased absorption of drugs. (3) Using a single nanoparticle formulation containing a drug mixture was frequently more effective than using a mixture of separate drugs [45]. This was because the nanoparticles facilitated the internalization of drugs into cells. By adopting this approach, drugs can enhance cellular effects more effectively and achieve synergy [42].

The distribution experiment accumulates AP and AD in numerous organs (the brain, kidney, liver, and heart). Further exploration was made to assess the safety of AP-AD PNPs in normal tissues. As expected, AP-AD PNPs showed promising safety without affecting normal tissues. Our findings indicate that AP-AD PNPs exhibit elevated levels of AP and AD in both rat plasma and heart compared to the AP&AD mixture. This can be attributed to their ability to mitigate the degradation of AP and AD effectively, extend the half-life of these substances, and reduce the rate at which they are cleared from the body. The study shows that AP-AD PNPs are more protective against MI injury. This was evidenced by the results of many tests, including histological inspection, TUNEL staining, measurement of myocardial enzyme-related and cardiac indexes, assessment of oxidative stress index, and evaluation of inflammatory index. The findings suggest that AP-AD PNPs can reduce MI harm caused by

doxorubicin (DOX) through anti-inflammatory, antioxidant, and anti-apoptotic mechanisms.

Conclusion

This investigation effectively fabricated AP-AD PNPs using the emulsion and microfluidic approach. In the formulation of the emulsion approach, AP and AD exhibited comparatively high EE and DL and small particle diameters. Significantly, the nanoparticles fabricated using emulsion exhibited superior stability and reduced viscosity despite the lesser polydispersity index (PDI) of the NPs prepared using the microfluidic approach. Subsequently, AP-AD PNPs, generated *via* emulsification, were employed in the subsequent pharmacokinetic and pharmacodynamic investigations. Pharmacokinetic tests demonstrated that AP-AD PNPs enhanced the stability of AP and AD, extended their duration in the bloodstream, lengthened the medicines' half-life, and reduced the rate at which they are cleared from the plasma. Furthermore, it improved the visibility of AP and AD within the cardiac system. Pharmacodynamic investigations, myocardial enzymes (AST, LDH, CK), oxidative stress (NO, GSH, MDA, SOD), and inflammation (TNF, IL-6) provided strong evidence to reveal that the treatment result of AP-AD PNPs in the DOX-induced MI was suggestively superior to that of AP&AD. It was found to be equivalent to the impact of the MT injection and had better anti-apoptosis capability. Overall, the AP-AD PNPs show potential as safe and effective drugs for treating MI.

Supplementary Information

The online version contains supplementary material available at <https://doi.org/10.1186/s12896-024-00912-y>.

Supplementary Material 1

Acknowledgements

The authors would like to thank all the members of our teams who helped in completing this work.

Author contributions

Ruixuan Li, Aixia Xu, Ye Chen: Conceptualization, Writing Original Draft, Data curation, Software, Writing Original Draft, Methodology, Analyzed and Interpreted the Data, Resources. Yihui Li, Ru Fu: Contributed Reagents, Materials, Analysis data, Software. Weihong Jiang, Xiaogang Li: Conceptualization, Writing - Review & Editing.

Funding

Not applicable.

Data availability

The datasets used and/or analysed during the current study are available from the corresponding author on reasonable request.

Declarations

Ethics approval and consent to participate

Primarily, adult male SPF rats (weight, 200–250 g; 10–12 weeks old; SLRC Laboratory Animal, Shanghai, China) were used to perform various *in vivo*

functional assessments. All animal procedures and protocols were approved by the animal centre of the Third Xiangya Hospital, Central South University and conformed to the "Guidelines for the Care and Use of Laboratory Animals" published by the U.S. NIH. Ethical approval for this study (Ethical No. 2023/2/BP) was obtained from the Ethics Committee of Central South University.

Consent for publication

Not applicable.

Competing interests

The authors declare no competing interests.

Received: 23 July 2024 / Accepted: 10 October 2024

Published online: 05 November 2024

References

1. Finegold JA, Asaria P, Francis DP. Mortality from ischaemic heart disease by country, region, and age: statistics from World Health Organisation and United Nations. *Int J Cardiol.* 2013;168:934–45.
2. Reed GW, Rossi JE, Cannon CP. Acute myocardial infarction. *Lancet.* 2017;389:197–210.
3. Anderson JL, Morrow DA. Acute myocardial infarction. *N Engl J Med.* 2017;376:2053–64.
4. Manson JE, Tosteson H, Ridker PM, Satterfield S, Hebert P, O'Connor GT, Buring JE, Hennekens CH. The primary prevention of myocardial infarction. *N Engl J Med.* 1992;326:1406–16.
5. Boateng S, Sanborn T. Acute myocardial infarction. *Dis DM.* 2013;59:83–96.
6. Wang X, Gao B, Feng Y. Recent advances in inhibiting atherosclerosis and restenosis: from pathogenic factors, therapeutic molecules to nano-delivery strategies. *J Mater Chem B.* 2022;10:1685–708.
7. Wang L, Ma Q. Clinical benefits and pharmacology of scutellarin: a comprehensive review. *Pharmacol Ther.* 2018;190:105–27.
8. Pala R, Anju VT, Dyavaiah M, Busi S, Nauli SM. Nanoparticle-mediated drug delivery for the treatment of cardiovascular diseases. *Int J Nanomed (2020)* 3741–69.
9. Karam M, Fahs D, Maatouk B, Safi B, Jaffa AA, Mhanna R. Polymeric nanoparticles in the diagnosis and treatment of myocardial infarction: challenges and future prospects. *Mater Today Bio.* 2022;14:100249.
10. Boarescu P-M, Boarescu I, Bocşan IC, Pop RM, Gheban D, Bulboacă AE, Nicula C, Răjnovăanu R-M, Bolboacă SD. Curcumin nanoparticles protect against isoproterenol induced myocardial infarction by alleviating myocardial tissue oxidative stress, electrocardiogram, and biological changes. *Molecules.* 2019;24:2802.
11. Khan S, Hasan A, Attar F, Sharifi M, Siddique R, Mraiche F, Falahati M. Gold nanoparticle-based platforms for diagnosis and treatment of myocardial infarction. *ACS Biomater. Sci Eng.* 2020;6:6460–77.
12. Chang M-Y, Yang Y-J, Chang C-H, Tang ACL, Liao W-Y, Cheng F-Y, Yeh C-S, Lai JJ, Stayton PS, Hsieh PCH. Functionalized nanoparticles provide early cardioprotection after acute myocardial infarction. *J Control Release.* 2013;170:287–94.
13. Bejarano J, Navarro-Marquez M, Morales-Zavala F, Morales JO, Garcia-Carvajal I, Araya-Fuentes E, Flores Y, Verdejo HE, Castro PF, Lavandero S, Kogan MJ. Nanoparticles for diagnosis and therapy of atherosclerosis and myocardial infarction: evolution toward prospective theranostic approaches. *Theranostics.* 2018;8:4710–32. <https://doi.org/10.7150/thno.26284>.
14. Pan Q, Xu J, Wen C-J, Xiong Y-Y, Gong Z-T, Yang Y-J. Nanoparticles: Promising Tools for the treatment and Prevention of myocardial infarction. *Int J Nanomed.* 2021;16:6719.
15. Simon-Yarza T, Tamayo E, Benavides C, Lana H, Formiga FR, Grama CN, Ortíz-de-Solorzano C, Kumar MNVR, Prosper F, Blanco-Prieto, functional benefits of PLGA particulates carrying VEGF and CoQ10 in an animal of myocardial ischemia. *Int J Pharm.* 2013;454:784–90.
16. Bei W, Jing L, Chen N. Cardio protective role of wogonin loaded nanoparticle against isoproterenol induced myocardial infarction by moderating oxidative stress and inflammation. *Colloids Surf B Biointerfaces.* 2020;185:110635.
17. Nagaoka K, Matoba T, Mao Y, Nakano Y, Ikeda G, Egusa S, Tokutome M, Nagahama R, Nakano K, Sunagawa K. A new therapeutic modality for acute myocardial infarction: nanoparticle-mediated delivery of pitavastatin induces cardioprotection from ischemia-reperfusion injury via activation of PI3K/Akt pathway and anti-inflammation in a rat model. *PLoS ONE.* 2015;10:e0132451.

18. Sun L, Hu Y, Mishra A, Sreeharsha N, Moktan JB, Kumar P, Wang L. Protective role of poly (lactic-co-glycolic) acid nanoparticle loaded with resveratrol against isoproterenol-induced myocardial infarction. *BioFactors*. 2020;46:421–31.
19. Xu J, Liu X, Zhang X, Qi K, Zha X. The Protective Effect and Mechanism of Apigenin in Myocardial Ischemia/Reperfusion Injury by Regulating AMPK/Nrf2/HO-1 Pathway, Reperfusion. *Inj. by Regul. AMPK/Nrf2/HO-1 Pathw.* (n.d.).
20. Alam W, Rocca C, Khan H, Hussain Y, Aschner M, De Bartolo A, Amodio N, Angelone T, Cheang WS. Current status and future perspectives on therapeutic potential of apigenin: focus on metabolic-syndrome-dependent organ dysfunction. *Antioxidants*. 2021;10:1643.
21. Li W, Chen L, Xiao Y. Apigenin protects against ischemia/hypoxia-induced myocardial injury by mediating pyroptosis and apoptosis. *Vitr Cell Dev Biol*. 2020;56:307–12.
22. Quan W, Ma S, Zhu Y, Shao Q, Hou J, Li X. Apigenin-7-O- β -d-(6"-p-coumaroyl)-glucopyranoside reduces myocardial ischaemia/reperfusion injury in an experimental model via regulating the inflammation response. *Pharm Biol*. 2020;58:80–8.
23. Thomas SD, Jha NK, Jha SK, Sadek B, Ojha S. Pharmacological and molecular insight on the cardioprotective role of apigenin. *Nutrients*. 2023;15:385.
24. Aetesam-ur-Rahman M, Brown AJ, Jaworski C, Giblett JP, Zhao TX, Braganza DM, Clarke SC, Agrawal BSK, Bennett MR, West NEJ. Adenosine-Induced Coronary Steal is observed in patients presenting with ST-Segment-elevation myocardial infarction. *J Am Heart Assoc*. 2021;10:e019899.
25. Laborante R, Bianchini E, Restivo A, Ciliberti G, Galli M, Vergallo R, Rodolico D, Zito A, Princi G, Leone AM. Adenosine as adjunctive therapy in acute coronary syndrome: a meta-analysis of randomized controlled trials. *Eur Hear Journal-Cardiovascular Pharmacother*. 2023;9:173–82.
26. Tallo FS, de Santana PO, Pinto SAG, Lima RY, De EA, Araújo JGP, Tavares M, Pires-Oliveira LAD, Nicolau JVR, Medeiros MO, Taha. Pharmacological modulation of the Ca²⁺/cAMP/Adenosine Signaling in Cardiac Cells as a New Cardioprotective Strategy to reduce severe arrhythmias in myocardial infarction. *Pharmaceuticals*. 2023;16:1473.
27. Sadeghian M, Mousavi SH, Aamarae Z, Shafiee A. Administration of intracoronary adenosine before stenting for the prevention of no-reflow in patients with ST-elevation myocardial infarction. *Scand Cardiovasc J*. 2022;56:23–7.
28. Procopio MC, Lauro R, Nasso C, Carerj S, Squadrito F, Bitto A, Di Bella G, Micari A, Irrera N, Costa F. Role of adenosine and purinergic receptors in myocardial infarction: focus on different signal transduction pathways. *Biomedicines*. 2021;9:204.
29. Hernández-Giottonini KY, Rodríguez-Córdova RJ, Gutiérrez-Valenzuela CA, Peñuñuri-Miranda O, Zavala-Rivera P, Guerrero-Germán P, Lucero-Acuña, PLGA nanoparticle preparations by emulsification and nanoprecipitation techniques: effects of formulation parameters. *RSC Adv*. 2020;10:4218–31. <https://doi.org/10.1039/C9RA10857B>.
30. Li T, Huang J, Wang M, Wang H. Microfluidic assembly of small-molecule prodrug cocktail nanoparticles with high reproducibility for synergistic combination of cancer therapy. *Int J Pharm*. 2021;608:121088. <https://doi.org/10.1016/j.ijpharm.2021.121088>.
31. Cotton DB, Lee W, Huhta JC, Dorman KF. Hemodynamic profile of severe pregnancy-induced hypertension. *Am J Obstet Gynecol*. 1988;158:523–9. [https://doi.org/10.1016/0002-9378\(88\)90017-8](https://doi.org/10.1016/0002-9378(88)90017-8).
32. Romano N, Ceci M. Are microRNAs responsible for cardiac hypertrophy in fish and mammals? What we can learn in the activation process in a zebrafish ex vivo model. *Biochim Biophys Acta - Mol Basis Dis*. 2020;1866:165896. <https://doi.org/10.1016/j.bbdis.2020.165896>.
33. Kosol W, Kumar S, Marrero-Berflos I, Berthiaume F. Medium conditioned by human mesenchymal stromal cells reverses low serum and hypoxia-induced inhibition of wound closure. *Biochem Biophys Res Commun*. 2019. <https://doi.org/10.1016/j.bbrc.2019.11.071>.
34. Alexiou S, Patoulias D, Theodoropoulos KC, Didagelos M, Nasoufidou A, Samaras A, Ziakas A, Fragakis N, Dardiotis E, Kassimis G. Intracoronary thrombolysis in ST-segment elevation myocardial infarction patients undergoing primary percutaneous coronary intervention: an updated meta-analysis of randomized controlled trials. *Cardiovasc. Drugs Ther*. 2024;38:335–46.
35. Kulick N, Friede KA, Stouffer GA. Safety and efficacy of intracoronary thrombolytic agents during primary percutaneous coronary intervention for STEMI. *Expert Rev. Cardiovasc Ther*. 2023;21:165–75.
36. Walters D, Mahmud E. Thrombolytic therapy for ST-elevation myocardial infarction presenting to non-percutaneous coronary intervention centers during the COVID-19 crisis. *Curr Cardiol Rep*. 2021;23:1–8.
37. Frangogiannis NG, Smith CW, Entman ML. The inflammatory response in myocardial infarction. *Cardiovasc Res*. 2002;53:31–47.
38. Jenča D, Melenovský V, Stehlik J, Staněk V, Kettner J, Kautzner J, Adámková V, Wohlfahrt P. Heart failure after myocardial infarction: incidence and predictors. *ESC Hear Fail*. 2021;8:222–37.
39. Wang Z, Long DW, Huang Y, Khor S, Li X, Jian X, Wang Y. Fibroblast growth Factor-1 released from a Heparin Coacervate improves cardiac function in a mouse myocardial infarction model. *ACS Biomater. Sci Eng*. 2017;3:1988–99. <https://doi.org/10.1021/acsbomaterials.6b00509>.
40. Zhang H, Chen H, Li J, Bian Y, Song Y, Li Z, He F, Liu S, Tsai Y. Hirudin protects against isoproterenol-induced myocardial infarction by alleviating oxidative via an Nrf2 dependent manner. *Int J Biol Macromol*. 2020;162:425–35. <https://doi.org/10.1016/j.ijbiomac.2020.06.097>.
41. Hou J, Wang C, Ma D, Chen Y, Jin H, An Y, Jia J, Huang L, Zhao H. The cardioprotective and anxiolytic effects of Chaihujiulonggumuli granule on rats with anxiety after acute myocardial infarction is partly mediated by suppression of CXCR4/NF- κ B/GSDMD pathway. *Biomed Pharmacother*. 2021;133:111015. <https://doi.org/10.1016/j.biopha.2020.111015>.
42. Li H, Xia B, Chen W, Zhang Y, Gao X, Chinnathambi A, Alharbi SA, Zhao Y. Nimbolide prevents myocardial damage by regulating cardiac biomarkers, antioxidant level, and apoptosis signaling against doxorubicin-induced cardiotoxicity in rats. *J Biochem Mol Toxicol*. 2020;34:e22543.
43. Hu C, Zhang X, Zhang N, Wei W, Li L, Ma Z, Tang Q. Osteocin attenuates inflammation, oxidative stress, apoptosis, and cardiac dysfunction in doxorubicin-induced cardiotoxicity. *Clin Transl Med*. 2020;10:e124.
44. He Y, Yang Z, Li J, Li E. Dexmedetomidine reduces the inflammation and apoptosis of doxorubicin-induced myocardial cells. *Exp Mol Pathol*. 2020;113:104371.
45. Hwang I, Uchida H, Dai Z, Li F, Sanchez T, Locasale JW, Cantley LC, Zheng H, Paik J. Cellular stress signaling activates type-I IFN response through FOXO3-regulated lamin posttranslational modification. *Nat Commun*. 2021;12:640. <https://doi.org/10.1038/s41467-020-20839-0>.

Publisher's note

Springer Nature remains neutral with regard to jurisdictional claims in published maps and institutional affiliations.